Dynamic estimation of soft tissue stiffness for use in modeling socket, orthosis or exoskeleton interfaces with lower limb segments

Sacha Guitteny, Yoann Lafon, Vincent Bonnet, Rachid Aissaoui, Raphaël Dumas

Dynamic estimation of soft tissue stiffness for use in modeling socket, orthosis or exoskeleton interfaces with lower limb segments

Sacha Guitteny, Yoann Lafon, Vincent Bonnet, Rachid Aissaoui, Raphael Dumas

PII: S0021-9290(22)00044-6
DOI: https://doi.org/10.1016/j.jbiomech.2022.110987
Reference: BM 110987

To appear in: *Journal of Biomechanics*

Received Date: 27 July 2021
Revised Date: 12 January 2022
Accepted Date: 1 February 2022

Please cite this article as: S. Guitteny, Y. Lafon, V. Bonnet, R. Aissaoui, R. Dumas, Dynamic estimation of soft tissue stiffness for use in modeling socket, orthosis or exoskeleton interfaces with lower limb segments, *Journal of Biomechanics* (2022), doi: https://doi.org/10.1016/j.jbiomech.2022.110987

Dynamic estimation of soft tissue stiffness for use in modeling socket, orthosis or exoskeleton interfaces with lower limb segments

Sacha Guitteny[a], Yoann Lafon[a], Vincent Bonnet[b], Rachid Aissaoui[c], Raphael Dumas[a]

[a]Univ Lyon, Univ Gustave Eiffel, LBMC UMR_T 9406, F-69622 Lyon, France

[b]LAAS/CNRS, Univ. Toulouse, F-31400, Toulouse, France

[c]Laboratoire de recherche en imagerie et orthopédie (LIO), Dépt Génie des systèmes, Ecole de technologie supérieure, Montréal, Canada

Article type : Original article

Correspondence:

Raphaël DUMAS

Telephone number: +33 4 72 14 23 56

Fax : +33 4 72 37 68 37

Email : raphael.dumas@univ-eiffel.fr

Word count from introduction to discussion : 3619

Abstract

Modeling the interface between the lower limb segments and a socket, orthosis or exoskeleton is crucial to the design, control, and assessment of such devices. The present study aimed to estimate translational and rotational soft tissue stiffness at the thigh and shank during daily living activities performed by six subjects.

Smooth orthogonal decomposition (SOD) was used on skin marker trajectories and fluoroscopy-based knee joint kinematics to compute stiffness coefficients during squatting, sitting and rising from a chair, level walking, and stair descending. On average, for all subjects and for all activities, in the anatomical directions observed, the translational and rotational stiffness coefficients for the shank were, respectively, 1.4±1.99kN/m (median and interquartile range) and 41.5±34.3Nm/deg. The results for the thigh segment were 1.79±2.73kN/m and 30.5±50.4Nm/deg.

As previously reported in the literature dealing with the soft tissue artifact – considered as soft tissue deformation in this study - the computed stiffness coefficients were dependent on tasks, subjects, segments, and anatomical directions. The main advantage of SOD over previous methods lies in enabling estimation of a task-dependent 6×6 stiffness matrix of the interface between segments and external devices, useful in their modeling and assessment.

Keywords

Soft tissue deformation, physical interface, segment compliance, motion capture, X-ray, total knee replacement, femur, tibia

Introduction

Multibody simulation is gaining popularity for the design and assessment of trans-tibial and trans-femoral prosthetic sockets (LaPrè et al., 2018; McGeehan et al., 2021; Pew et al., 2020), rehabilitation knee orthoses (Arch et al., 2016; Ebert et al., 2014; Hall et al., 2019; Mouzo et al., 2020), and passive or active exoskeletons (Chander and Cavatorta, n.d.; Fournier et al., 2018; Gordon et al., 2018; Serrancoli et al., 2019; Torricelli et al., 2018; Uchida et al., 2016; Zhang et al., 2021). Unfortunately, however, little is known about the effects of loadings from external devices on the musculoskeletal system (Asbeck et al., 2015). Defining the interface between the thigh and shank segments and the assistive device (socket, orthosis or exoskeleton) is an important step in modeling. In this field of application, soft tissues are characterized as linear springs, with stiffness at this interface assumed negligible or infinite (Grabke et al., 2019) according to different authors. In other words, depending on the anatomical direction, the assistive device can either move freely or is totally constrained (and can therefore entirely transmit the external forces and moments produced by the device). Yet few models introduce arbitrary stiffness coefficients at the interface (Gordon et al., 2018; Lim et al., 2016; McGeehan et al., 2021), although a good knowledge of these stiffness-related parameters is required for effective modeling.

The stiffness of the soft tissue plays an important role in the comfort and the performance of the assistive device (Cherry et al., 2016; Shafiei and Behzadipour, 2020a; Yandell et al., 2017). Recent studies have attempted to address this through forward simulations, identifying spring parameter values at the interface (Mouzo et al., 2020; Serrancoli et al., 2019). However, these studies only used unidimensional springs that do not adequately represent the true mechanical behavior of the interface. From an experimental point of view, soft tissue stiffness has also been estimated mainly in a single anatomical direction at

a time, using indentation methods (Daley et al., 1993; Erickson et al., 1993; Liu et al., 1995). These methods computed stiffness coefficients in a static condition, the subject being seated and relaxed. A recent study (Shafiei and Behzadipour, 2020b) estimated the thigh and shank 6×6 stiffness matrices based on data from three subjects, but still in a static and relaxed condition. Another use of the soft tissue stiffness parameter has been to model wobbling mass and to analyze its impact on whole body dynamics (Alonso et al., 2007; Gittoes et al., 2006; Gruber et al., 1998; Pain and Challis, 2004). In this perspective, smooth orthogonal decomposition (SOD) was applied to skin and pin data from four subjects to estimate translational stiffness during walking, hopping, cutting, and running (Dumas and Jacquelin, 2017). The authors suggest that this method can be extended to estimate rotational stiffness and to study dynamic activities that are more representative of daily living in a rehabilitation context.

Thus, the aim of this study was to estimate translational and rotational soft tissue stiffness of the thigh and shank. Data from the literature provided the movements of skin markers relative to their underlying bones (Taylor et al., 2017). From the kinematics point of view, this deformation is generally considered as a soft tissue artifact. However, it can be viewed as relevant (Camomilla et al., 2017) to assessing the wobbling mass effect and, in the present case, estimating stiffness at the interface between the skeleton and an assistive device. The authors hypothesize that the translational and rotational stiffness estimated by SOD during squatting, sitting and rising from a chair, level walking, and stair descending is consistent with the stiffness coefficients at the interface between lower limb segments and assistive devices already reported in the literature. The aims of this work are (i) to investigate whether SOD offers a viable alternative method of characterizing the interface in

dynamic conditions, (ii) to confirm that static and dynamic evaluations provide comparable results, and (iii) to extend the estimation of soft tissue stiffness to different subjects and tasks.

Material and methods

Dataset and processing

The experimental data for this study were taken from Taylor et al. (2017) (Taylor et al., 2017) (https://cams-knee.orthoload.com/). This dataset gave access to fluoroscopic data (25Hz) and skin marker positions (VICON, 100Hz) for 6 subjects (5 males and 1 female, 68 ± 5years, 88 ± 12kg, 1.73 ± 0.04m) wearing a knee prosthesis while performing daily living activities: squatting, sitting and rising from a chair, level walking, and stair descending. Each subject performed these activities once and was equipped with a set of 8 skin markers on the shank segment and 10 skin markers on the thigh segment: markers were placed on medial, lateral, frontal and ventral sides. Fluoroscopy-based kinematics concerned the implant coordinate system (CS), while skin marker trajectories were from the laboratory CS. All transformation matrices between the different CS and CT-Scan anatomical landmarks were provided by the authors.

The raw data on skin marker position were gap-filled using QTM (Qualisys Track Manager) software. Polynomial interpolations were used when the gap was no longer than 0.1s (10 frames), and the “relational/rigid body” method otherwise. The anatomical landmark positions enabled the anatomical CS of both shank and thigh segments to be defined according to the International Society of Biomechanics (ISB)(Wu et al., 2002). The origins of both thigh and shank anatomical CSs were defined at the knee joint center (mid-point between medial and lateral femoral epicondyles in the CT-Scan acquisition). The

fluoroscopic data were up-sampled to 100Hz (frequency of the VICON system) using quaternion (*slerp*) interpolation. A reference position for each skin marker was defined as the mean position in the anatomical CS during all movements. The gait data for patient 2 were excluded due to apparently inconsistent movement of the skin markers relative to their underlying bones.

Smooth orthogonal decomposition (SOD)

SOD of skin marker movement relative to underlying bones was used to compute the translational stiffness of the soft tissues of both thigh and shank segments during the dynamic activities. This involved defining a soft tissue artifact (STA) vector $\mathbf{v}$, representing the displacement of the skin markers relative to the reference position in the anatomical CS (Dumas et al., 2014) (Figure 1). This vector was projected on the three anatomical directions to define the amplitudes of movements *a* of the rigid clusters of markers for both thigh and shank segments, in translation (Eq. 1):

$$a_i^l(k) = \{\mathbf{\Phi}_i^l\}^T \mathbf{V}_i(k) \ \#(Eq.\ 1)$$

$$\text{with } \mathbf{\Phi}_i^1 = \begin{pmatrix} \vdots \\ 1/\sqrt{m_i} \\ 0 \\ 0 \\ \vdots \end{pmatrix}, \ \mathbf{\Phi}_i^2 = \begin{pmatrix} \vdots \\ 0 \\ 1/\sqrt{m_i} \\ 0 \\ \vdots \end{pmatrix}, \text{ and } \mathbf{\Phi}_i^3 = \begin{pmatrix} \vdots \\ 0 \\ 0 \\ 1/\sqrt{m_i} \\ \vdots \end{pmatrix} \qquad \text{(Eq.2)}$$

where $\left\{\mathbf{\Phi}_i^l\right\}$ (l = 1, 2, 3) are the unitary basis vectors built a priori to define the three translations of the marker cluster of segment *i* about, respectively, the X, Y, and Z axis of its anatomical CS. Superscript *T* denotes transpose of the basis vector and m_i is the number of skin markers on segment *i*. Because the data from the monoplane fluoroscope could not be

considered fully reliable in the medial-lateral direction, the results along this direction were not analyzed.

The stiffness matrix $\mathbf{K}_i$ (dimension 3 × 3) was then computed for the thigh and shank segments, defining the stiffness along the smooth orthogonal vectors. Indeed, the stiffness coefficients are the solution of an eigen-problem representing free undamped vibrations of a cluster of lumped masses (Dumas and Jacquelin, 2017) (Appendix B). Assuming that movement amplitude depends on free undamped vibrations of a cluster of lumped masses, the smooth orthogonal modes are good estimates of the linear normal modes and correspond to anatomical directions. The masses M_i assigned to the shank and thigh soft tissues (i.e. skin, adipose tissue, and muscle) were estimated as 4.8% and 12.3% of the total body (Dumas et al., 2007) and 77.65% and 90.3% of the segment (Clarys and Marfell-Jones, 1986), respectively.

This method was extended in the present study to compute the stiffness coefficients corresponding to each of the marker-cluster rotations. For this purpose, three additional unitary basis vectors were defined representing the marker-cluster rotations around the origin and about the axes of the anatomical CS:

$$\left\{\boldsymbol{\Phi}_i^4 \quad \boldsymbol{\Phi}_i^5 \quad \boldsymbol{\Phi}_i^6\right\} = \left[\frac{\boldsymbol{L}_i}{det\,(\boldsymbol{L}_i)}\right]\left\{\boldsymbol{\Phi}_i^1 \quad \boldsymbol{\Phi}_i^2 \quad \boldsymbol{\Phi}_i^3\right\} \qquad \text{(Eq. 3)}$$

$$\text{with } \mathbf{L}_i = \begin{bmatrix} \ddots & & \\ & \tilde{\mathbf{L}}_i^j & \\ & & \ddots \end{bmatrix} \text{ and } \tilde{\mathbf{L}}_i^j = \begin{bmatrix} 0 & -\mathbf{r}_i^j z & \mathbf{r}_i^j y \\ \mathbf{r}_i^j z & 0 & -\mathbf{r}_i^j x \\ -\mathbf{r}_i^j y & \mathbf{r}_i^j x & 0 \end{bmatrix} \qquad \text{(Eq. 4)}$$

where $\tilde{\boldsymbol{L}}_i^j$is the skew matrix of the reference position $\mathbf{r}_i^j$ of skin marker *j* of segment *i* in the anatomical CS (Figure 1) and det($\mathbf{L}_i$) is the determinant of matrix $\mathbf{L}_i$. This formulation is based on the relationship (lever arm) between the force applied at one skin marker and the related moment at the origin of the anatomical CS or, similarly, on the relationship between

the linear displacement of one skin marker and the related rotation of the marker cluster around the origin. Only the stiffness parameters in flexion-extension and internal-external rotations were analyzed in this study, since the data from the monoplane fluoroscope could not reliably be applied to abduction-adduction.

Results

For all subjects, anatomical directions, and activities, the translational and rotational stiffness coefficients were in the range of [0.18 – 4.77kN/m] and [13.4 – 85.7Nm/deg] for the shank and of [0.17 – 16.9kN/m] and [2.6 - 231Nm/deg] for the thigh. Figures 2 and 3 compare, respectively, the translational and rotational stiffness for all activities to the stiffness coefficients reported in the literature (Daley et al., 1993; Karlsson and Tranberg, 1999; Kuiken et al., 2018; Lim et al., 2016; Liu et al., 1995; Mouzo et al., 2020; Pew et al., 2020; Shafiei and Behzadipour, 2020b).

The stiffness coefficients calculated via SOD were higher for the shank than for the thigh during the less dynamic activities (squatting and sitting/rising from a chair): 1.39kN/m and 41.5 Nm/deg for the shank against 0.89kN/m and 17.6kN/deg for the thigh, on average, along the different anatomical directions (supplementary figures S1 and S2). However, this difference in stiffness coefficients was not observed for more dynamic activities. Moreover, the thigh soft tissue stiffness coefficients for squatting and sitting/rising from a chair were similar to each other (0.7±1.2kN/m and 17.7±16.9Nm/deg), with higher stiffness coefficients for walking and stair descending (2.61±3.4kN/m and 67.1±55.8kN/deg). As shown in Table 1, there was significant inter-subject variability for both segments. In particular, the maximum standard deviations (std) for the translational and the rotational stiffness parameters were

found during stair descending (std = 2.14kN/m and std = 36.8Nm/deg for the shank, std = 3.69kN/m and std = 47.8N/deg for the thigh).

Discussion

The objective of this study was to estimate translational and rotational stiffness of the thigh and shank during daily living activities. SOD was used to compute stiffness coefficients about various axes of the anatomical CS, revealing heterogeneity among tasks, subjects, segments, and directions. The results of this study are consistent with the literature documenting the dependency of the STA on all these factors (Camomilla et al., 2017; Leardini et al., 2005; Peters et al., 2010). (Asbeck et al., 2015) also conclude that soft tissue stiffness is dependent on the location where it is estimated (anchoring points of the exoskeleton) and on the direction (normal or tangential to the bone segment). This study did not estimate extra-diagonal terms of the stiffness matrix accordingly to the study of (Shafiei and Behzadipour, 2020b) that claims the stiffness matrix to be almost diagonal in the anatomical directions.

It should be noted that SOD differs from other methods of computing stiffness coefficients, which analyze the linear force-displacement relationship. SOD analyzes free undamped vibrations of a cluster of lumped masses. It was hypothesized that the stiffness of the STA estimated by SOD would be consistent with that estimated at the interface between lower limb segments and assistive device and reported in the literature. Our results partially support this claim. Some studies (Daley et al., 1993; Liu et al., 1995; Shafiei and Behzadipour, 2020b) have used indentation or instrumented exoskeleton cuffs to estimate translational stiffness coefficients of the thigh and shank. Applying the indentation method to the thigh soft tissues (Daley et al., 1993; Liu et al., 1995) yielded stiffness coefficients of between 1.43kN/m and 3.28kN/m. Mouzo et al. (2020)(Mouzo et al., 2020) suggested using

springs connecting the skeleton to an orthosis to simulate gait, and identified these stiffnesses: 2.5kN/m and 2.8kN/m for the upper and mid-thigh, respectively, and 9.8kN/m for the upper shank. Furthermore, (Karlsson and Tranberg, 1999) investigated local translational stiffness parameters along both shank and thigh segments by applying a load to an adhesive tape attached to the skin in anterior-posterior and proximal-distal directions. The resulting stiffness parameters were 0.7kN/m and 1.4kN/m on average for the shank along the anterior-posterior and the proximal-distal directions, respectively, and 0.5kN/m and 0.7kN/m for the thigh. The translational stiffness coefficients found via SOD are of the same order of magnitude for both segments (Figure 2). In Shafiei and Behzadipour (2020)(Shafiei and Behzadipour, 2020b), the lowest translational stiffness coefficients found along the longitudinal direction for both segments were 3.3kN/m and 1.4kN/m, respectively, for shank and thigh. Similarly, the stiffness coefficients obtained via SOD along the anterior-posterior direction (2.18kN/m and 2.83kN/m on average for shank and thigh, respectively) were higher than those in the longitudinal direction (0.84kN/m and 1.01kN/m for shank and thigh, respectively). Yet there remain differences between the stiffness coefficients calculated in this study and those found by indentation or instrumented exoskeleton cuffs (Daley et al., 1993, 1993; Liu et al., 1995; Shafiei and Behzadipour, 2020b), especially for rotational stiffness. One explanation could be that the STA represents mainly the behavior of the skin, while other methods explore deeper and stiffer tissues due to penetration by the indenter (Fougeron et al., 2020) and tightening of the cuffs. Moreover, the method detailed in this study analyzes skin marker movements for entire segments, while other methods focus on more local behavior at the anchoring points of the external device.

Few studies have sought to characterize the rotational stiffness coefficients. Shafiei and Behzadipour (2020)(Shafiei and Behzadipour, 2020b) defined 6×6 stiffness matrices for both thigh and shank segments. Pew et al. (2020)(Pew et al., 2020) estimated rotational stiffness coefficients of the shank using inverse kinematics and inverse dynamics at the socket-residual limb interface (modeled as a 4-DoF joint) in transtibial amputees during three different dynamic activities. While Pew et al. (2020)(Pew et al., 2020) found rotational stiffness coefficients (0.45±0.1Nm/deg along the longitudinal direction of the shank segment) of the same order of magnitude as Shafiei and Behzadipour (2020)(Shafiei and Behzadipour, 2020b), SOD yielded higher coefficients than those reported by either of these two studies (Figure 3). Finally, Kuiken et al. (2018)(Kuiken et al., 2018), reporting frontal and sagittal rotational stiffness coefficients for the thigh based on a transfemoral amputee patient's volitional socket loading, recorded an average sagittal rotation stiffness (along Z axis) of 5.6Nm/deg, comparable to the SOD-computed coefficients for sitting/rising from a chair. Apart from methodological differences in stiffness computation, the observed difference might be due to different muscular contraction or external loadings (static conditions vs. dynamic movements, relaxed vs. contracted muscles). Indeed, Fougeron et al. (2020)(Fougeron et al., 2020) highlighted differences in the stiffness of thigh soft tissues between relaxed and contracted muscle states. Such stiffness differences were also observed by (Karlsson and Tranberg, 1999) for shank segments, with an increase of 0.4kN/m on average in anterior-posterior direction and of 0.3KN/m in proximal-distal direction. Unfortunately, no details are provided by Shafiei and Behzadipour (2020) on degree of muscular contraction (Shafiei and Behzadipour, 2020b), nor in the literature reporting translational stiffness (Daley et al., 1993; Karlsson and Tranberg, 1999; Liu et al., 1995).

As mentioned above when comparing translational stiffness findings, the numerical approach selected here relies on a cluster of markers distributed homogeneously around the segments. Other approaches estimating the stiffness coefficients at the interface alone (Shafiei and Behzadipour, 2020b) therefore naturally define the rotation differently: rotations around the exoskeleton cuff (Shafiei and Behzadipour, 2020b) or the center of the socket (Pew et al., 2020). The present study chose the knee joint center to provide stiffness coefficients (Table 1), as a well-defined and more convenient situation for motion analysis and musculoskeletal modeling. For the same reason, the stiffness coefficients computed in this study are expressed using the CS as standardized by the ISB. Finally, Pew et al. (2020) (Pew et al., 2020) and Mouzo et al. (2020) (Mouzo et al., 2020) estimated stiffness coefficients via numerical approaches like inverse and forward dynamics and reported stiffness coefficients corresponding to the extreme values documented here, the minimum and the maximum, respectively. Some arbitrary defined stiffness coefficients (McGeehan et al., 2021) even reached the maximum value of 20kN/m and the minimum value of 0.01Nm/deg (these values were not displayed for readability of Figure 2 and 3).

This study has some limitations. First, the approach is sensitive to experimental set-up, and the number and location of skin markers may affect results. For this reason, the present study considered the amplitude of translation and rotation of the whole marker cluster (Appendix B). Nevertheless, the set of markers needs to be distributed homogeneously on each segment and their number large enough to properly describe the complex STA pattern revealed by Barré et al. (2017)(Barré et al., 2017), in all anatomical directions. The CAMS-Knee dataset used here includes 8 and 10 markers placed around the entire circumference of the thigh and shank segments, respectively. To define the STA vector, marker displacement should be measured relative to underlying bones. The present study relied on

already published data using mono-plane fluoroscopy: the 2D/3D registration error of the implant CAD model was reported to be less than 1 degree for all rotations, less than 1 mm and 3 mm for in- and out-of-plane translations, respectively (Taylor et al., 2017). Moreover, fluoroscope acquisition frequency was only 25Hz, whereas Wakeling et al (2003) (Wakeling et al., 2003) found greater frequencies at heel strike for soft tissue vibration with respect to the ground. However, during an entire gait cycle, the STA (soft tissue vibration with respect to the underlying bone) lies in a frequency band of 0 – 10Hz (Bonci et al., 2014). (Murphy, 1990) studied thigh and shank frequencies (in both translations and rotations) during gait, using intracortical pin and skin markers, and also found a frequency band of under 8Hz. Thus, working at 25Hz can be considered appropriate here (Nyquist-Shannon sample-rate criterion), since gait is the most dynamic movement studied.

It is also worth noting that this numerical approach based on motion capture is subject to experimental errors in the marker trajectories, for example due to occlusion (Conconi et al., 2021), or more precisely to the gap-filling method used to solve these occlusions. As described by (Guitteny et al., 2021), the soft tissue stiffness parameters resulting from the vibrational analysis are bound to differ for a population wearing an external device, due to added mass or tissue compression, for example. A final limitation is that only six subjects' data were available and analyzed in this study. However, given their age, these subjects can be expected to be representative of a population likely to wear an orthosis or an exoskeleton. The performance of this SOD method could be further assessed by comparing it to several methods widely used in literature (like indentation), on a given set of subjects and under as rich an experimental set-up as this one.

The SOD method presented in this study offers an original approach to estimating soft tissue stiffness. It was previously used to characterize the wobbling mass effect in hopping,

cutting, and running (Dumas and Jacquelin, 2017) and provides a way of estimating the components of the forces and moments at the interface (not studied here). Soft tissue deformation may be influenced by movements like squatting, sitting/ rising from a chair, level walking, and stair descending, and therefore static evaluation – as previously by indentation (Daley et al., 1993; Erickson et al., 1993; Liu et al., 1995; Shafiei and Behzadipour, 2020b) – is not appropriate to account for this task-dependency. Consistent with Pew et al. (2020)(Pew et al., 2020), this study revealed a task-dependent stiffness at the interface between lower limb segments and assistive device. Together with the developing fluoroscopic analysis of the STA, both for various activities and segments (Akbarshahi et al., 2010; Barre et al., 2013; D'Isidoro et al., 2020; Fiorentino et al., 2020; Kuo et al., 2011; Tsai et al., 2009) and for socket or orthosis interactions with segments (Gale et al., 2020; Papaioannou et al., 2010), the proposed SOD method may pave the way to new approaches that more finely evaluate soft tissue stiffness in all anatomical directions during different dynamic activities. For instance, as reported in Richard et al. (2016) (Richard et al., 2016) for the knee joint, the deformation energy at the interface between skeleton and assistive device can be calculated from stiffness coefficients and minimized to perform advanced inverse kinematics. Adding the forces and moments generated by the assistive device's movements relative to the skeleton to the orthosis abduction moment (Brandon et al., 2019) can better represent the device's mechanics. In forward simulation, the unidirectional spring (Lim et al., 2016; Mouzo et al., 2020; Serrancoli et al., 2019) can now be replaced by 3 translational and 3 rotational springs, with the same aim of modeling the interface between skeleton and assistive device more realistically.

To conclude, this study extended the application of the SOD method to the STA, using it to compute translational and rotational stiffness coefficients for skin marker movement relative to fluoroscopy-based kinematics during daily living dynamic activities in six subjects. The computed stiffness coefficients were found to depend on the tasks, subjects, segments, and anatomical directions. Estimated values for the translational stiffness coefficients were of the same order of magnitude as those reported in the literature, while those for the rotational stiffness coefficients were higher, possibly due to different degrees of tissue depth and stiffness, different muscular activation levels, and/or different external loadings. Being able to compute stiffness coefficients should improve the design, modeling and control of socket, orthosis or exoskeleton. Taking into account stiffness at the interface between the body segment and the assistive device should help to limit compression and shear forces and improve its performance and comfort.

Acknowledgement

This study was performed within the framework of the LABEX PRIMES (ANR-11-LABX-0063) of Université de Lyon, under the program ‘‘Investissements d’Avenir” (ANR-11-IDEX-0007) operated by the French National Research Agency (ANR).

Conflict of interest statement

The authors do not have any financial or personal relationships with other people or organizations that would have inappropriately influenced this study.

References

Akbarshahi, M., Schache, A.G., Fernandez, J.W., Baker, R., Banks, S., Pandy, M.G., 2010. Non-invasive assessment of soft-tissue artifact and its effect on knee joint kinematics during functional activity. Journal of Biomechanics 43, 1292–1301. https://doi.org/10.1016/j.jbiomech.2010.01.002

Alonso, F.J., Del Castillo, J.M., Pintado, P., 2007. Motion data processing and wobbling mass modelling in the inverse dynamics of skeletal models. Mechanism and Machine Theory 42, 1153–1169. https://doi.org/10.1016/j.mechmachtheory.2006.08.006

Arch, E.S., Stanhope, S.J., Higginson, J.S., 2016. Passive-dynamic ankle–foot orthosis replicates soleus but not gastrocnemius muscle function during stance in gait: Insights for orthosis prescription. Prosthet Orthot Int 40, 606–616. https://doi.org/10.1177/0309364615592693

Asbeck, A.T., De Rossi, S.M.M., Holt, K.G., Walsh, C.J., 2015. A biologically inspired soft exosuit for walking assistance. The International Journal of Robotics Research 34, 744–762. https://doi.org/10.1177/0278364914562476

Barré, A., Aissaoui, R., Aminian, K., Dumas, R., 2017. Assessment of the lower limb soft tissue artefact at marker-cluster level with a high-density marker set during walking. Journal of Biomechanics 62, 21–26. https://doi.org/10.1016/j.jbiomech.2017.04.036

Barre, A., Thiran, J.-P., Jolles, B.M., Theumann, N., Aminian, K., 2013. Soft Tissue Artifact Assessment During Treadmill Walking in Subjects With Total Knee Arthroplasty. IEEE Trans. Biomed. Eng. 60, 3131–3140. https://doi.org/10.1109/TBME.2013.2268938

Bonci, T., Camomilla, V., Dumas, R., Chèze, L., Cappozzo, A., 2014. A soft tissue artefact model driven by proximal and distal joint kinematics. Journal of Biomechanics 47, 2354–2361. https://doi.org/10.1016/j.jbiomech.2014.04.029

Brandon, S.C.E., Brown, M.J., Clouthier, A.L., Campbell, A., Richards, J.D., Deluzio, K.J., 2019. Contributions of muscles and external forces to medial knee load reduction due to osteoarthritis braces. The Knee 26, 564–577. https://doi.org/10.1016/j.knee.2019.04.006

Camomilla, V., Dumas, R., Cappozzo, A., 2017. Human movement analysis: The soft tissue artefact issue. Journal of Biomechanics 62, 1–4. https://doi.org/10.1016/j.jbiomech.2017.09.001

Chander, D.S., Cavatorta, M.P., n.d. Modelling friction at the mechanical interface between the human and the exoskeleton 18.

Cherry, M.S., Kota, S., Young, A., Ferris, D.P., 2016. Running With an Elastic Lower Limb Exoskeleton. Journal of Applied Biomechanics 32, 269–277. https://doi.org/10.1123/jab.2015-0155

CLARYS, J.P., MARFELL-JONES, M.J., 1986. Anthropometric Prediction of Component Tissue Masses in the Minor Limb Segments of the Human Body. Human Biology 58, 761–769.

Conconi, M., Pompili, A., Sancisi, N., Parenti-Castelli, V., 2021. Quantification of the errors associated with marker occlusion in stereophotogrammetric systems and implications on gait analysis. Journal of Biomechanics 114, 110162. https://doi.org/10.1016/j.jbiomech.2020.110162

Daley, B.J., Ralston, J.L., Brown, T.D., Brand, R.A., 1993. A Parametric Design Evaluation of Lateral Prophylactic Knee Braces. Journal of Biomechanical Engineering 115, 131–136. https://doi.org/10.1115/1.2894112

D'Isidoro, F., Brockmann, C., Ferguson, S.J., 2020. Effects of the soft tissue artefact on the hip joint kinematics during unrestricted activities of daily living. Journal of Biomechanics 104, 109717. https://doi.org/10.1016/j.jbiomech.2020.109717

Dumas, R., Camomilla, V., Bonci, T., Cheze, L., Cappozzo, A., 2014. Generalized mathematical representation of the soft tissue artefact. Journal of Biomechanics 47, 476–481. https://doi.org/10.1016/j.jbiomech.2013.10.034

Dumas, R., Chèze, L., Verriest, J.-P., 2007. Adjustments to McConville et al. and Young et al. body segment inertial parameters. Journal of Biomechanics 40, 543–553. https://doi.org/10.1016/j.jbiomech.2006.02.013

Dumas, R., Jacquelin, E., 2017. Stiffness of a wobbling mass models analysed by a smooth orthogonal decomposition of the skin movement relative to the underlying bone. Journal of Biomechanics 62, 47–52. https://doi.org/10.1016/j.jbiomech.2017.06.002

Ebert, J.R., Hambly, K., Joss, B., Ackland, T.R., Donnelly, C.J., 2014. Does an Unloader Brace Reduce Knee Loading in Normally Aligned Knees? Clin Orthop Relat Res 472, 915–922. https://doi.org/10.1007/s11999-013-3297-8

Erickson, A.R., Yasuda, K., Beynnon, B., Johnson, R., Pope, M., 1993. An in vitro dynamic evaluation of prophylactic knee braces during lateral impact loading. Am J Sports Med 21, 26–35. https://doi.org/10.1177/036354659302100105

Fiorentino, N.M., Atkins, P.R., Kutschke, M.J., Bo Foreman, K., Anderson, A.E., 2020. Soft tissue artifact causes underestimation of hip joint kinematics and kinetics in a rigid-body musculoskeletal model. Journal of Biomechanics 108, 109890. https://doi.org/10.1016/j.jbiomech.2020.109890

Fougeron, N., Rohan, P.-Y., Hearing, D., Rose, J.-L., Bonnet, X., Pillet, H., 2020. 1 Combining Freehand Ultrasound-Based 2 Indentation and Inverse Finite Element 3 Modelling for the Identification of Hyperelastic 4 Material Properties of Thigh Soft Tissues 22.

Fournier, B.N., Lemaire, E.D., Smith, A.J.J., Doumit, M., 2018. Modeling and Simulation of a Lower Extremity Powered Exoskeleton. IEEE Trans. Neural Syst. Rehabil. Eng. 26, 1596–1603. https://doi.org/10.1109/TNSRE.2018.2854605

Gale, T., Yang, S., McGough, R., Fiedler, G., Anderst, W., 2020. Motion of the residual femur within the socket during gait is associated with patient-reported problems in transfemoral amputees. Journal of Biomechanics 112, 110050. https://doi.org/10.1016/j.jbiomech.2020.110050

Gittoes, M.J.R., Brewin, M.A., Kerwin, D.G., 2006. Soft tissue contributions to impact forces simulated using a four-segment wobbling mass model of forefoot–heel landings. Human Movement Science 25, 775–787. https://doi.org/10.1016/j.humov.2006.04.003

Gordon, D.F.N., Henderson, G., Vijayakumar, S., 2018. Effectively Quantifying the Performance of Lower-Limb Exoskeletons Over a Range of Walking Conditions. Front. Robot. AI 5, 61. https://doi.org/10.3389/frobt.2018.00061

Grabke, E.P., Masani, K., Andrysek, J., 2019. Lower Limb Assistive Device Design Optimization Using Musculoskeletal Modeling: A Review. Journal of Medical Devices 13, 040801. https://doi.org/10.1115/1.4044739

Gruber, K., Ruder, H., Denoth, J., Schneider, K., 1998. A comparative study of impact dynamics: wobbling mass model versus rigid body models. Journal of Biomechanics 6.

Guitteny, S., Dumas, R., Lafon, Y., n.d. A reduced finite element model for virtual prototyping of knee orthosis. COMPUTER METHODS IN BIOMECHANICS AND BIOMEDICAL ENGINEERING 3.

Hall, M., Diamond, L.E., Lenton, G.K., Pizzolato, C., Saxby, D.J., 2019. Immediate effects of valgus knee bracing on tibiofemoral contact forces and knee muscle forces. Gait & Posture 68, 55–62. https://doi.org/10.1016/j.gaitpost.2018.11.009

Karlsson, D., Tranberg, R., 1999. On skin movement artefact-resonant frequencies of skin markers attached to the leg. Human Movement Science 18, 627–635. https://doi.org/10.1016/S0167-9457(99)00025-1

Kuiken, T.A., Fey, N.P., Reissman, T., Finucane, S.B., Dumanian, G.A., 2018. Innovative Use of Thighplasty to Improve Prosthesis Fit and Function in a Transfemoral Amputee: Plastic and Reconstructive Surgery - Global Open 6, e1632. https://doi.org/10.1097/GOX.0000000000001632

Kuo, M.-Y., Tsai, T.-Y., Lin, C.-C., Lu, T.-W., Hsu, H.-C., Shen, W.-C., 2011. Influence of soft tissue artifacts on the calculated kinematics and kinetics of total knee replacements during sit-to-stand. Gait & Posture 33, 379–384. https://doi.org/10.1016/j.gaitpost.2010.12.007

LaPrè, A.K., Price, M.A., Wedge, R.D., Umberger, B.R., Sup, F.C., 2018. Approach for gait analysis in persons with limb loss including residuum and prosthesis socket dynamics. Int J Numer Meth Biomed Engng 34, e2936. https://doi.org/10.1002/cnm.2936

Leardini, A., Chiari, L., Croce, U.D., Cappozzo, A., 2005. Human movement analysis using stereophotogrammetry. Gait & Posture 21, 212–225. https://doi.org/10.1016/j.gaitpost.2004.05.002

Lim, B., Hyung, S., Kim, K., Lee, J., Jang, J., Shim, Y., 2016. Simulating gait assistance of a hip exoskeleton: Feasibility studies for ankle muscle weaknesses, in: 2016 IEEE/RSJ International Conference on Intelligent Robots and Systems (IROS). Presented at the 2016 IEEE/RSJ International Conference on Intelligent Robots and Systems (IROS), IEEE, Daejeon, South Korea, pp. 5664–5669. https://doi.org/10.1109/IROS.2016.7759833

Liu, S., Daluiski, A., Kabo, M., 1995. The effect of thigh soft-tissue stiffness on the control of anterior tibial displacement by function knee orthosis.pdf. Journal of Rehabilitation Research and Development 32, 135–140.

McGeehan, M.A., Adamczyk, P.G., Nichols, K.M., Hahn, M.E., 2021. A Computational Gait Model With a Below-Knee Amputation and a Semi-Active Variable-Stiffness Foot Prosthesis. Journal of Biomechanical Engineering 143, 124502. https://doi.org/10.1115/1.4052108

Mouzo, F., Michaud, F., Lugris, U., Cuadrado, J., 2020. Leg-orthosis contact force estimation from gait analysis. Mechanism and Machine Theory 148, 103800. https://doi.org/10.1016/j.mechmachtheory.2020.103800

Murphy, M.C., 1990. Geometry and the kinematics of the normal human knee.

Pain, M.T.G., Challis, J.H., 2004. Wobbling Mass Influence on Impact Ground Reaction Forces: A Simulation Model Sensitivity Analysis. Journal of Applied Biomechanics 20, 309–316. https://doi.org/10.1123/jab.20.3.309

Papaioannou, G., Mitrogiannis, C., Nianios, G., Fiedler, G., 2010. Assessment of amputee socket–stump–residual bone kinematics during strenuous activities using Dynamic Roentgen Stereogrammetric Analysis. Journal of Biomechanics 8.

Peters, A., Galna, B., Sangeux, M., Morris, M., Baker, R., 2010. Quantification of soft tissue artifact in lower limb human motion analysis: A systematic review 8.

Pew, C.A., Roelker, S.A., Klute, G.K., Neptune, R.R., 2020. Analysis of the Relative Motion Between the Socket and Residual Limb in Transtibial Amputees While Wearing a Transverse Rotation Adapter. Journal of Applied Biomechanics 1–9. https://doi.org/10.1123/jab.2019-0362

Serrancoli, G., Falisse, A., Dembia, C., Vantilt, J., Tanghe, K., Lefeber, D., Jonkers, I., De Schutter, J., De Groote, F., 2019. Subject-Exoskeleton Contact Model Calibration Leads to Accurate Interaction Force Predictions. IEEE Trans. Neural Syst. Rehabil. Eng. 27, 1597–1605. https://doi.org/10.1109/TNSRE.2019.2924536

Shafiei, M., Behzadipour, S., 2020a. Adding backlash to the connection elements can improve the performance of a robotic exoskeleton. Mechanism and Machine Theory 152, 103937. https://doi.org/10.1016/j.mechmachtheory.2020.103937

Shafiei, M., Behzadipour, S., 2020b. The Effects of the Connection Stiffness of Robotic Exoskeletons on the Gait Quality and Comfort. Journal of Mechanisms and Robotics 12, 011007. https://doi.org/10.1115/1.4044841

Taylor, W.R., Schütz, P., Bergmann, G., List, R., Postolka, B., Hitz, M., Dymke, J., Damm, P., Duda, G., Gerber, H., Schwachmeyer, V., Hosseini Nasab, S.H., Trepczynski, A., Kutzner, I., 2017. A comprehensive assessment of the musculoskeletal system: The CAMS-Knee data set. Journal of Biomechanics 65, 32–39. https://doi.org/10.1016/j.jbiomech.2017.09.022

Torricelli, D., Cortés, C., Lete, N., Bertelsen, Á., Gonzalez-Vargas, J.E., del-Ama, A.J., Dimbwadyo, I., Moreno, J.C., Florez, J., Pons, J.L., 2018. A Subject-Specific Kinematic Model to Predict Human Motion in Exoskeleton-Assisted Gait. Front. Neurorobot. 12, 18. https://doi.org/10.3389/fnbot.2018.00018

Tsai, T.-Y., Lu, T.-W., Kuo, M.-Y., Hsu, H.-C., 2009. QUANTIFICATION OF THREE-DIMENSIONAL MOVEMENT OF SKIN MARKERS RELATIVE TO THE UNDERLYING BONES DURING FUNCTIONAL ACTIVITIES. Biomed. Eng. Appl. Basis Commun. 21, 223–232. https://doi.org/10.4015/S1016237209001283

Uchida, T.K., Seth, A., Pouya, S., Dembia, C.L., Hicks, J.L., Delp, S.L., 2016. Simulating Ideal Assistive Devices to Reduce the Metabolic Cost of Running. PLoS ONE 11, e0163417. https://doi.org/10.1371/journal.pone.0163417

Wakeling, J.M., Liphardt, A.-M., Nigg, B.M., 2003. Muscle activity reduces soft-tissue resonance at heel-strike during walking. Journal of Biomechanics 36, 1761–1769. https://doi.org/10.1016/S0021-9290(03)00216-1

Wu, G., Siegler, S., Allard, P., Kirtley, C., Leardini, A., Rosenbaum, D., Whittle, M., D'Lima, D.D., Cristofolini, L., Witte, H., Schmid, O., Stokes, I., 2002. ISB recommendation on definitions of joint coordinate system of various joints for the reporting of human joint motion—part I: ankle, hip, and spine. Journal of Biomechanics 35, 543–548. https://doi.org/10.1016/S0021-9290(01)00222-6

Yandell, M.B., Quinlivan, B.T., Popov, D., Walsh, C., Zelik, K.E., 2017. Physical interface dynamics alter how robotic exosuits augment human movement: implications for optimizing wearable assistive devices. J NeuroEngineering Rehabil 14, 40. https://doi.org/10.1186/s12984-017-0247-9

Zhang, L., Liu, Y., Wang, R., Smith, C., Gutierrez-Farewik, E.M., 2021. Modeling and Simulation of a Human Knee Exoskeleton's Assistive Strategies and Interaction. Front. Neurorobot. 15, 620928. https://doi.org/10.3389/fnbot.2021.620928

Table & figure captions:

Table 1: Median, inter-quartile range, minimal and maximal translational and rotational stiffness coefficients computed via SOD during activities (squatting, sitting and rising from a chair, level walking, and stair descending).

Figure 1: Sagittal view of the thigh and shank skin marker displacements with respect to femoral and tibial implants and anatomical landmarks of both segments for one subject (KL1) and one task (sitting and rising from a chair). HJC: hip joint center, LFE: lateral femoral epicondyle, MFE: medial femoral epicondyle, KJC: knee joint center, LM: lateral malleolus, MM: medial malleolus, $\mathbf{r}_i^j$: reference position of skin marker *j* of segment *i* in the anatomical CS, $\mathbf{v}_i^j(k)$: displacement of skin markers *j* of segment *i* at sampled instant of time *k* relative to the reference position in the anatomical CS.

Figure 2: Translational stiffness coefficients computed via SOD during all dynamic activities, compared to literature values.

Figure 3: Rotational stiffness coefficients computed via SOD during all dynamic activities, compared to literature values.

Table 1

				All activities	**Squatting**	**Sitting/Rising from a chair**	**Level walking**	**Stair descending**
Translational stiffness coefficient (kN/m)	**Shank**	X	Median (IQR) [Min ; Max]	2.18 (1.98) [0.71 ; 4.77]	3.03 (0.99) [1.59 ; 4.21]	1.24 (0.81) [0.71 ; 2.67]	1.86 (2.53) [1.1 ; 4.42]	1.97 (1.96) [1 ; 4.77]
		Y	Median (IQR) [Min ; Max]	0.84 (1.36) [0.18 ; 3.32]	0.94 (1.59) [0.49 ; 2.61]	0.56 (0.86) [0.18 ; 1.91]	1.27 (1.08) [0.43 ; 2.35]	0.88 (1.55) [0.21 ;3.32]
		Mean (X and Y)	Median (IQR) [Min ; Max]	1.4 (1.99) [0.18 ; 4.77]	2.35 (2.09) [0.49 ; 4.21]	1.02 (0.83) [0.18 ; 2.67]	1.57 (1.25) [0.43 ;4.42]	1.42 (2.14) [0.21 ; 4.77]
	Thigh	X	Median (IQR) [Min ; Max]	2.83 (4.59) [0.38 ; 16.9]	2.39 (3.79) [0.49 ; 8.07]	0.9 (1.78) [0.38 ; 4.21]	5.21 (4.25) [3.1 ; 8.94]	4.39 (7.09) [1.82 ; 16.9]
		Y	Median (IQR) [Min ; Max]	1.01 (1.3) [0.17 ; 5.26]	0.45 (0.22) [0.17 ; 0.88]	0.59 (0.38) [0.33 ; 0.97]	1.76 (0.44) [1.06 ; 2.01]	2.47 (1.38) [1.38 ; 5.26]
		Mean (X and Y)	Median (IQR) [Min ; Max]	1.79 (2.73) [0.17 ; 16.9]	0.75 (1.95) [0.17 ; 8.07]	0.7 (0.45) [0.33 ; 4.21]	2.56 (3.45) [1.06 ; 8.95]	2.61 (3.69) [1.38 ; 16.9]

Table 1 - following

Rotational stiffness coefficient (Nm/deg)	**Shank**	Y	Median (IQR) [Min ; Max]	41.5 (36.1) [19 ; 82.7]	54.9 (26) [20.4 ; 82.7]	27.9 (15.3) [19 ; 41.5]	59.6 (30.4) [23.9 ; 66.5]	43.1 (40.2) [20.2 ; 78.8]
		Z	Median (IQR) [Min ; Max]	39.5 (28) [13.4 ; 85.7]	49.3 (15) [32.2 ; 73.2]	22.8 (14.2) [13.4 ; 48.9]	33 (50.9) [18.9 ; 80.3]	40 (25.6) [17.9 ; 85.7]
		Mean (Y and Z)	Median (IQR) [Min ; Max]	41.5 (34.3) [13.4 ; 85.7]	49.3 (22.1) [20.4 ; 82.7]	25.4 (12.9) [13.4 ; 48.9]	46.5 (35.6) [18.9 ; 80.3]	40 (36.8) [17.9 ; 85.7]
	Thigh	Y	Median (IQR) [Min ; Max]	29.5 (49.2) [4 ; 111]	20.6 (13.8) [12.7 ; 57.6]	16.9 (10.7) [4 ; 19.1]	67.2 (23.4) [26.4 ; 112]	47.8 (38.8) [28.9 ; 70.7]
		Z	Median (IQR) [Min ; Max]	34.5 (71.7) [2.6 ; 231]	19 (30.8) [2.9 ; 97.1]	5.6 (15.4) [2.6 ; 29.6]	76.2 (55.9) [30.3 ; 111]	67.5 (58.8) [32.6 ; 231]
		Mean (Y and Z)	Median (IQR) [Min ; Max]	30.5[(50.4) [2.6 ; 231]	19.2 (18.7) [2.9 ; 97.1]	12.5 (12.5) [2.6 ; 29.6]	68.6 (47.4) [26.4 ; 112]	55.7 (47.8) [28.9 ; 231]

Figure 1

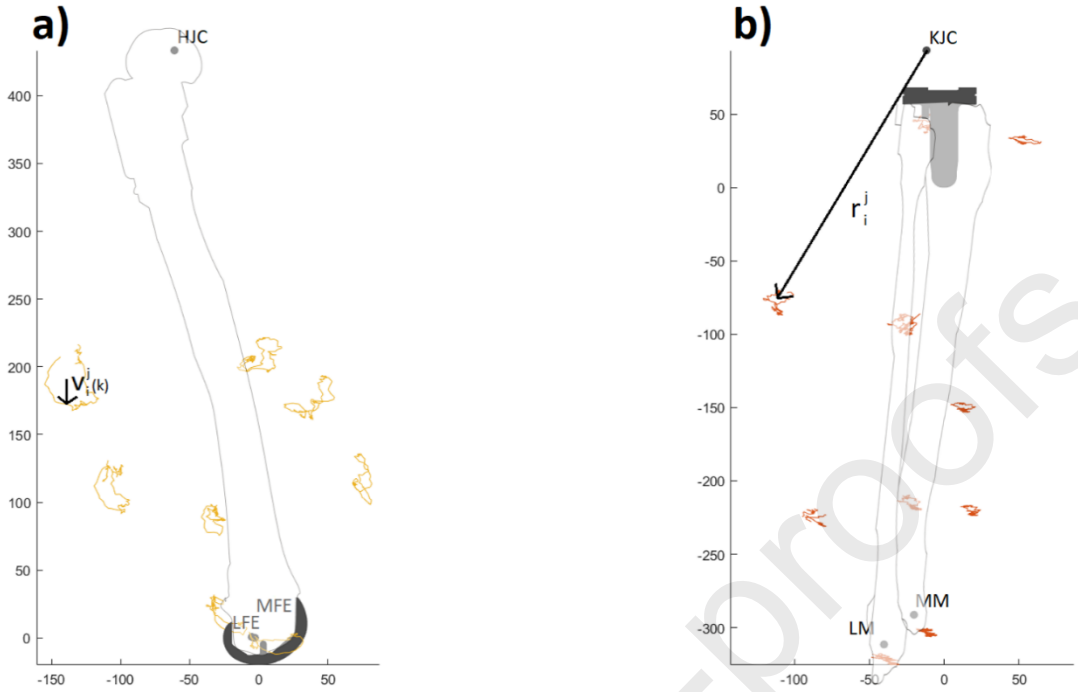

Figure 2

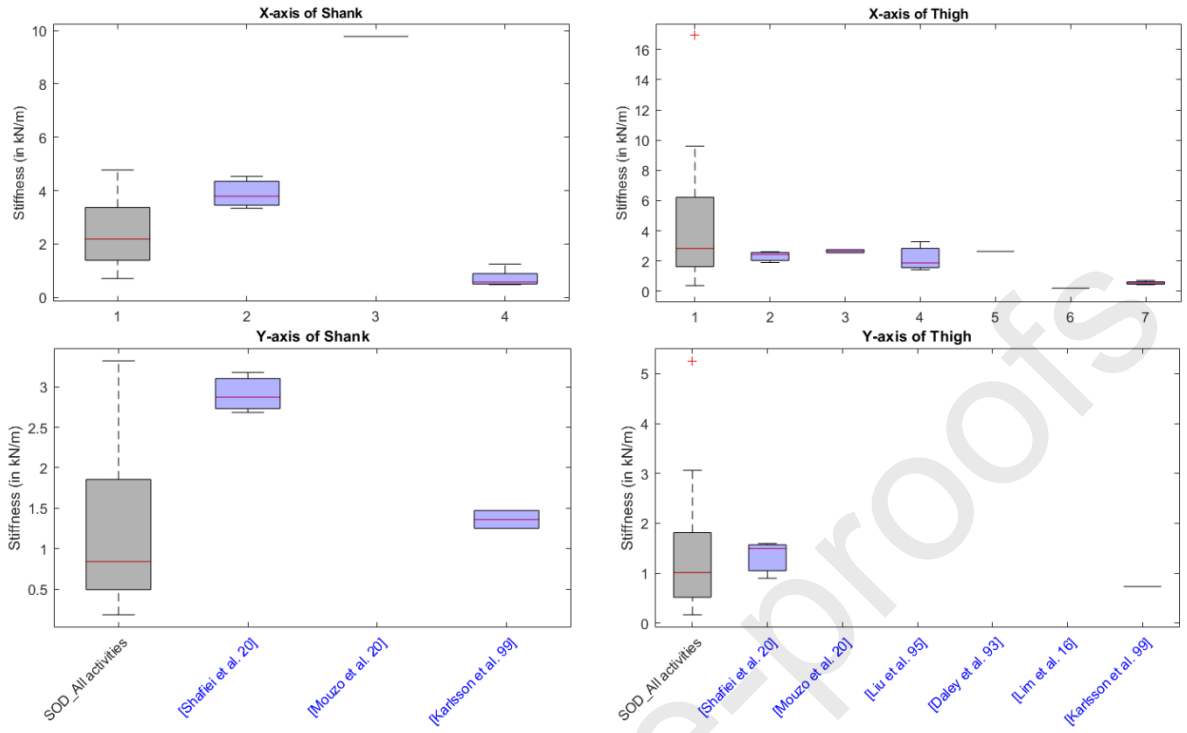

Figure 3

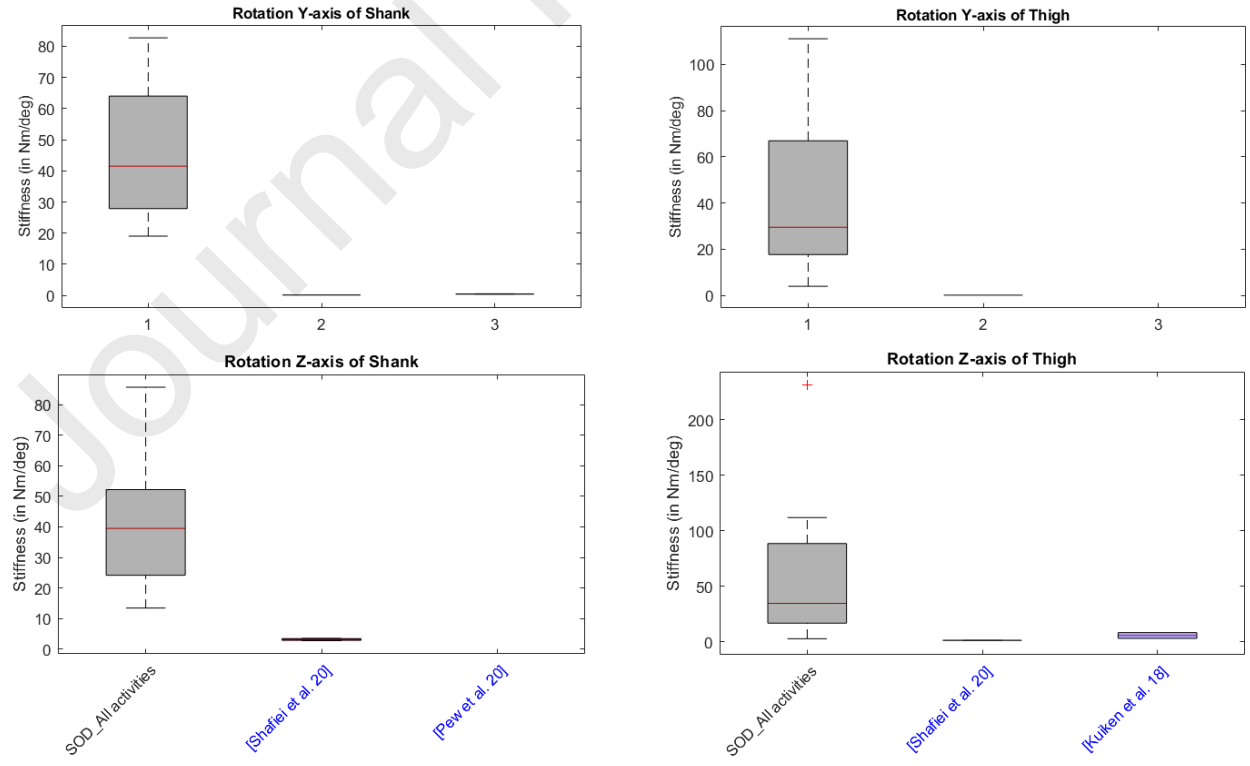

Appendix A – Nomenclature

Nomenclature			
i	Index for segment	$\mathbf{U}$	Velocity covariance matrix (3 × 3)
j	Index for skin marker	$\mathbf{\Psi}$	Smooth orthogonal vector (3*n × 3)
k	Index for sampled instant of time	λ, $\boldsymbol{\lambda}$	Smooth orthogonal value, diagonal matrix of eigenvalues (3 × 3)
n	Number of sampled instants of time	ω	Frequency
m	Number of markers on a segment	$\mathbf{K}$	Stiffness matrix (3×3)
$\mathbf{r}$	Reference position of skin marker	M	Mass
$\mathbf{v}$, $\mathbf{V}$	STA vector, STA field (3m*n × 1)	$\mathbf{\Phi}$	Basis vector (i.e. marker cluster geometrical transformation) (3m*n × 3)
$\mathbf{S}$	Sample covariance matrix (3×3)	$\tilde{\mathbf{L}}$	Screw matrix (3×3)
$\mathbf{D}$	Differential operator (n-1 × n)	a	Modal amplitude (n × 3)
f	Sampling frequency		

Appendix B – SOD method, proposed by Dumas et Jacquelin (2017)(Dumas and Jacquelin, 2017) **and adapted in the present study (*)**

The STA of all markers on the segment *i* were represented using the STA field, $\mathbf{V}_i(k)$:

$$\mathbf{V}_i(k) = \begin{pmatrix} \vdots \\ \mathbf{v}_i^j(k) \\ \vdots \end{pmatrix} \#(1)$$

(*) Movement amplitudes *a* of the marker clusters of both thigh and shank segments were computed:

$$a_i^l(k) = \{\mathbf{\Phi}_i^l\}^T \mathbf{V}_i(k) \ \#(2)$$

The covariance matrix was computed from these amplitudes (rather than directly from the STA field*) known at every sampled instant of time:

$$\mathbf{S}_i = \frac{1}{n}\{\cdots \quad a_i^l(k) \quad \cdots\}\{\cdots \quad a_i^l(k) \quad \cdots\}^T \#(3)$$

(*) Amplitudes of movement $a_i^l(k)$ in translations and in rotations cannot be processed at the same time since the unitary basis vectors $\mathbf{\Phi}_i^l$ are not orthogonal.

In the smooth orthogonal decomposition, a differential operator was further introduced:

$$\mathbf{D} = f\begin{bmatrix} -1 & 1 & 0 & \cdots & 0 \\ 0 & -1 & 1 & \cdots & 0 \\ \vdots & \ddots & \ddots & \ddots & 0 \\ 0 & \ldots & 0 & -1 & 1 \end{bmatrix} \#(4)$$

where *f* was the sampling frequency.

This differential operator allowed the computation of the other covariance matrix standing for the velocities of the cluster of skin markers:

$$\mathbf{U}_i = \frac{1}{n-1}\mathbf{D}\{\cdots \quad a_i^l(k) \quad \cdots\}\{\cdots \quad a_i^l(k) \quad \cdots\}^T[\mathbf{D}]^T \#(5)$$

The smooth orthogonal modes were solutions of the eigen-problem:

$$\mathbf{S}_i\left[\cdots \quad \boldsymbol{\Psi}_i^l \quad \cdots\right] = \boldsymbol{\lambda}_i \mathbf{U}_i\left[\cdots \quad \boldsymbol{\Psi}_i^l \quad \cdots\right] \#(6)$$

with $\boldsymbol{\Psi}_i^l$ (l = 1:3) the smooth orthogonal vectors and $\boldsymbol{\lambda}_i$ a diagonal matrix composed of the smooth orthogonal eigenvalues of which$\left(\omega_i^l\right)^2 = \left(\lambda_i^l\right)^{-1}$are the circular frequencies related to the smooth orthogonal values. Assuming that the movement amplitudes resulted from free undamped vibrations of lumped masses M_i at the barycentre of the cluster of markers, the stiffness matrix $\mathbf{K}_i$ was given by:

$$\mathbf{K}_i = M_i\left[\cdots \quad \boldsymbol{\Psi}_i^l \quad \cdots\right]\left[\boldsymbol{\lambda}_i\right]^{-1}\left[\cdots \quad \boldsymbol{\Psi}_i^l \quad \cdots\right]^{-1} \#(7)$$

Supplementary material

Figure S1: Translational stiffness coefficients computed via SOD during dynamic activities (squatting, sitting and rising from a chair, level walking, and stair descending), compared to literature values.

Figure S2: Rotational stiffness coefficients computed via SOD during dynamic activities (squatting, sitting and rising from a chair, level walking, and stair descending), compared to literature values

Figure S1

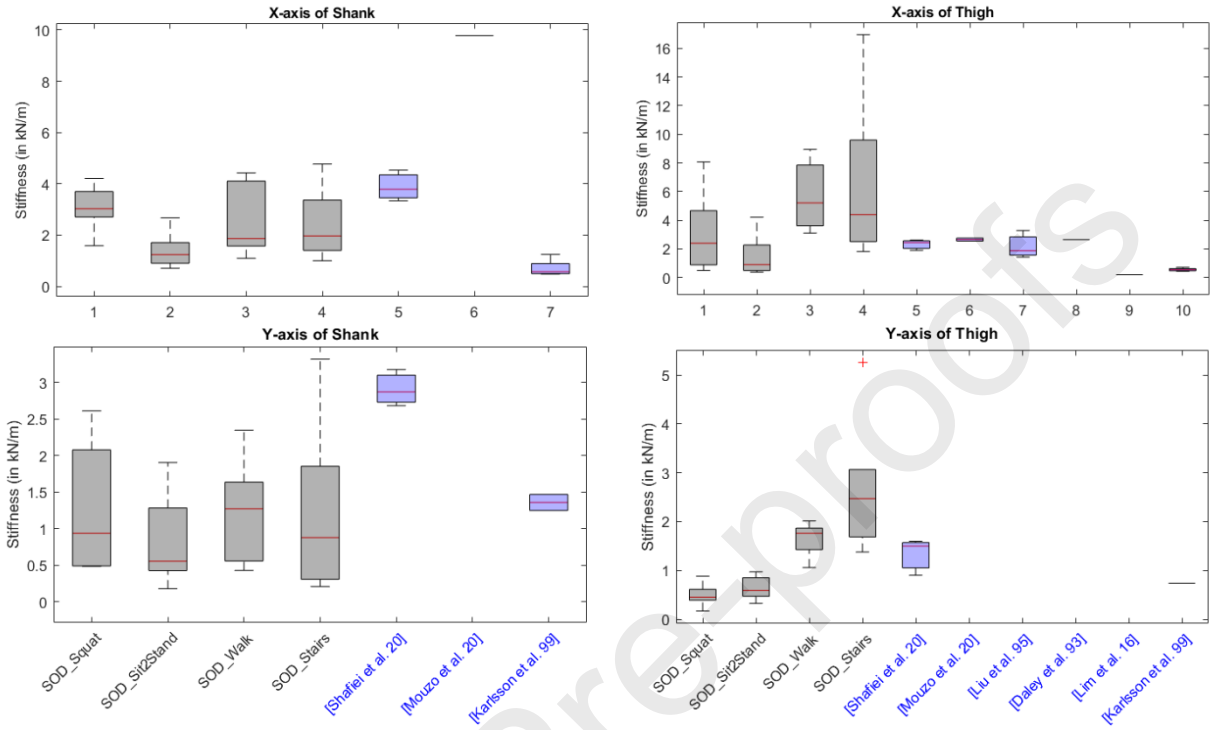

Figure S2